The Canadian Mineralogist
Vol. 44, pp. 795-810 (2006)

REDOX AND SPECIATION OF TIN IN HYDROUS SILICATE GLASSES: A COMPARISON WITH Nb, Ta, Mo AND W

FRANÇOIS FARGES§

Laboratoire de Minéralogie (USM 201), Muséum National d'Histoire Naturelle, CNRS UMR 7160, 61, rue Buffon, F–75005 Paris, France, and Department of Geological and Environmental Sciences, Stanford University, Stanford, California 94305–2115, USA

ROBERT L. LINNEN

Department of Earth Sciences, University of Waterloo, Waterloo, Ontario N2L 3G1, Canada

GORDON E. BROWN JR.

Department of Geological and Environmental Sciences, Stanford University, Stanford, California 94305–2115, and Stanford Synchrotron Radiation Laboratory, Stanford University, Stanford, California 94305–2115, USA

ABSTRACT

The speciation of tin in nine hydrous haplogranitic silicate glasses (0.1–1 wt.% SnO_2) was investigated by XAFS spectroscopy at the tin *K*-edge. Three compositions of granitic melt were investigated [peralkaline (ASI 0.6), metaluminous (ASI 1.0), and peraluminous (ASI 1.2)] and, for each of these, tin-bearing glasses were synthesized at three different redox conditions (~FMQ, ~FMQ + 1.1, and ~FMQ + 2.4). The hydrous glasses were quenched from H_2O-saturated melts at 850°C and 2 kbar. Redox states estimated from XANES are in good agreement with those estimated from SnO_2 dissolution experiments. There are, however, some unresolved discrepancies. Tetravalent Sn is dominant in all peralkaline melts investigated, even at FMQ. In contrast, Sn(II) is dominant in the peraluminous compositions investigated, even at FMQ + 2.4. The tin *K*-edge XAFS spectra for the oxidized glasses resemble that of eakerite [$Ca_2SnAl_2Si_6O_{18}(OH)_2 \bullet 2H_2O$]. Tetravalent Sn thus behaves in a similar manner to Zr(IV), a network modifier, but is markedly different from Ti(IV), a network former. In the most reduced glasses, highly ionic Sn(II)-bearing moieties are formed. Thus, Sn(II) is comparable to Ca^{2+}, *i.e.*, it is an efficient network modifier, in sharp contrast to Sn(IV). Consequently, Sn(IV) is soluble in silicate melts that contain non-bridging oxygen (NBO) atoms, such as peralkaline compositions. In contrast, in peraluminous magmas, in which NBO are lacking, Sn(II) preferentially forms highly ionic moieties that can be easily "complexed" and transported by, for instance, chlorine. If the redox conditions become oxidizing, Sn(IV) forms, but cannot accommodate itself within the framework of tetrahedra of the melt structure, which results in nucleation of cassiterite. In a comparison of speciation information for Nb(V), Ta(V), W(VI) and Mo(VI) in similar compositions of glass, Sn(IV) acts more like Nb(V), Ta(V) or Zr(IV), whereas Mo(VI) and W(VI) form highly covalent complexes (*sensu stricto*) that are disconnected from the framework of tetrahedra. Tin geochemistry in melts appears to be dominated by an exchange between two highly different structural positions for Sn(IV) and Sn(II), which is highly sensitive to peralkalinity under conditions of moderate fugacity of oxygen. In contrast, the mineralogy of tin is dominated by Sn(IV). The difference in the valence of tin in melts vs minerals makes it a very unusual cation as compared to other highly charged cations to which tin is commonly associated, such as Mo, W, Ta and Nb.

Keywords: tin, hydrous glasses, XAFS spectroscopy, solubility, highly charged cations.

SOMMAIRE

La spéciation de l'étain dans neuf verres silicatés (0.1–1% SnO_2, poids) a été examinée par spectroscopie XAFS au seuil *K* de l'étain. Chacune des trois compositions étudiées [hyperalcaline (ASI 0.6), méta-alumineuse (ASI 1.0) et hyperalumineuse (ASI 1.2)] a été synthétisée sous trois conditions redox différentes (~FMQ, ~FMQ + 1.1 et ~FMQ + 2.4). Les verres ont été trempés depuis des magmas saturés en H_2O à 850°C et 2 kbar. L'état redox mesuré par XANES est en général cohérent avec l'état mesuré grâce à la dissolution de SnO_2. Le Sn(IV) domine dans les verres hyperalcalins, même à FMQ + 2.4. Au contraire,

§ *E-mail address*: francoisfarges@gmail.com

le Sn(II) domine dans les verres hyperalumineux, même à FMQ + 2.4. Les spectres XAFS des verres riches en Sn(IV) ressemblent à ceux de l'eakerite [$Ca_2SnAl_2Si_6O_{18}(OH)_2$•$2H_2O$]. Ainsi, Sn(IV) se comporte alors comme Zr(IV), donc comme un modificateur de réseau, et diffère de Ti(IV), qui est un formateur de réseau. Dans les verres réduits, le Sn(II) forme des unités ioniques, se comportant alors comme un modificateur de réseau efficace (tout comme Na^+). Le Sn(IV) est très soluble dans les magmas silicatés tant que des atomes d'oxygène non-pontants (ONP) existent, comme dans les compositions hyperalcalines. Dans des magmas hyperalumineux, appauvris en ONP, le Sn(II) est stabilisé sous forme d'unités ioniques, qui peuvent être alors facilement complexées et transportées par du chlore. Si les conditions redox redeviennent oxydantes, le Sn(IV) est restabilisé, mais ce dernier ne peut plus être accommodé dans le réseau de tétraèdres du magma, provoquant alors une nucléation de cassitérite. Pour comparer, des informations de spéciation ont été obtenues pour Nb(V), Ta(V), W(VI) et Mo(VI) dans des conditions similaires. Sn(IV) est proche de Nb(V), de Ta(V) ou de Zr(IV), alors que Mo(VI) et W(VI) forment des unités très covalentes et déconnectées du réseau tétraèdrique. Ainsi, la géochimie de l'étain dans les magmas semble dominée par l'ambivalence entre deux états redox (II, IV) au comportement structural très différents mais dominé par Sn(II), alors que sa mineralogie est dominée par Sn(IV). Ceci rend l'étain très particulier par rapport aux autres cations fortement charges avec lequel il est souvent associé comme Mo, W, Ta and Nb.

Mots-clés : étain, verres hydratés, spectroscopie XAFS, solubilité, cations fortement chargés.

Introduction

Divalent tin is a highly incompatible "granitophile" and lithophile element (Taylor 1979, Eugster 1985) that concentrates into late-stage magmas (*e.g.*, those enriched in Li, Be and B and depleted in alkaline earths; Tischendorf 1977) and magmatic-hydrothermal fluids in natural alkaline, subaluminous or peraluminous granitic systems (see Lehmann 1990 for a review). Tungsten, niobium and tantalum also concentrate in such magmas. In contrast, tetravalent tin is more compatible, as it substitutes for Ti^{4+} in minerals such as magnetite and titanite, and thus typically is not concentrated in more oxidized, evolved granitic melts (Lehmann 1990, Linnen 1998). Experimental studies (Linnen *et al.* 1995, 1996, Ellison et al. 1998, Bhalla et al. 2005) have focused on the solubility, diffusivity and mobilization of tin in both hydrous and anhydrous systems. A growing body of evidence suggests that the behavior of tin in such melts is highly dependent on the alkalinity [or 1/ASI, where ASI is the aluminum saturation index, *i.e.*, the molar ratio Al/[Na + K]), as well as the abundances of volatile phases (*e.g.*, F, Cl). Tin complexation by chlorine is now well established for hydrothermal fluids (*e.g.*, Sherman *et al.* 2000, Seby *et al.* 2001), but very few investigators have provided direct information on the redox state of tin in glasses (Durasova *et al.* 1986, 1997, Music *et al.* 1991, Taylor & Wall 1992), and there are no studies on the speciation of tin in silicate glasses of geochemical interest.

Previous investigators have used ^{119}Sn Mössbauer spectroscopy to obtain redox information on tin in glasses (Durasova *et al.* 1986, 1997, Music et al. 1991, Taylor & Wall 1992). In this study, we utilize XAFS spectroscopy to provide, for the first time, some direct information on the speciation and coordination geochemistry of tin in H_2O-saturated alkaline, metaluminous and peraluminous haplogranitic melts, in order to better understand the speciation of tin in natural magmatic systems. This information is compared to that measured for other anhydrous silicate glasses of similar composition containing Nb, Ta, Mo or W. However, tin *K*-edge XAFS spectroscopy is challenging because of the relatively high energy required to collect the *K*-edge information (26200 eV). At these energies, most synchrotron sources emit much less intense X-rays. Also, experimental resolution is limited owing to both the relatively large core-hole lifetime of the tin *K*-edge (~6 eV) and the use of relatively low monochromator angles (below 10°). These difficulties, in theory, could be overcome by collecting XAFS information at the tin *L*-edges (3929–4465 eV). These experiments failed, however, because of experimental problems associated with data collection at these relatively low energies, particularly in K-rich compositions that contain dilute concentrations of tin (below 1000 ppm). An additional problem is that the potassium *K*-edge is located right below the L_{III}-edge of tin (3608 and 3929 eV, respectively), making the collection of L_{III}-edge tin EXAFS spectra challenging without using a highly sensitive energy-discriminant solid-state detector (that was not available). In addition, the L_{II} and L_I edges are located at higher energies (4156 and 4465 eV, respectively), but their fluorescence yield is too low for the dilute concentrations of tin in the glasses studied here. Also, these *L*-edges are very sensitive to absorption of moisture (to within a few micrometers of the surface), which can provide information on relaxed structures, but these spectra are not characteristic of the bulk glasses, the description of which is the goal of this study.

Experimental

Model compounds

The Sn-bearing crystals investigated included cassiterite crystals (SnO_2; two gemmy crystals, one from Bolivia and one from gravels in Malaysia [crystal-structure information taken from Seki *et al.* (1984) at 295 K], eakerite [$Ca_2SnAl_2Si_6O_{18}(OH)_2$•$2H_2O$; the cotype specimen from the Foote mine, North Carolina, USA; crystal-structure information from Kossiakoff &

Leavens 1976], two perovskite-structure polymorphs (orthorhombic) synthesized at 1500°C for 3 hours ($SnSrO_3$, $CaSnO_3$; Widera & Schaefer 1981, Vallet-Regi *et al*. 1986), $CdSn(OH)_6$, romarchite (SnO, rutile modification; XAFS data courtesy of Giefers & Wortmann 2002; crystal-structure information from Pannetier & Denes 1980), $SnCl_2$ (kept solid below 10°C during data collection; crystal-structure information from Léger & Haines 1996), and metallic tin (to calibrate the *K*-edge of tin at 29200 eV). In addition to synthetic metallic foils, models for W and Ta include a sample of hübnerite, $(Mn_{0.7}Fe_{0.3})WO_4$, from Montebras, Creuse, France), scheelite ($CaWO_4$; from Salau, Pyrénées, France), tantalite [$(Fe,Mn)(Ta,Nb)_2O_6$, from Amelia, Virginia, USA; Nb_2O_5 content of 10 wt.%) and columbite–tantalite ("coltan" from the Shaba region in the Democratic Republic of Congo, with 9.1 and 8.8 wt.% FeO and MnO, respectively). Models for Mo (including powellite, wulfenite, and molybdenite) are described elsewhere (Farges *et al*. 2006). The Malaysian cassiterite and the molybdenite samples are from the Stanford University mineral collection; the other samples are minerals from the first author's collection. Romarchite, the three perovskite crystals and the Cd–Sn hydroxide were synthesized from reagent-grade chemicals. All samples were characterized by optical or X-ray emission and X-ray diffraction, as well as by electron-microprobe analysis.

Hydrous silicate glasses

The glasses studied were quenched from H_2O-saturated melts at 850°C and 2 kbar. Three haplogranitic compositions (in the system quartz – albite – orthoclase) were investigated: peralkaline (ASI 0.6), metaluminous (ASI 1.0) and peraluminous (ASI 1.2). One series of glasses (SQ) were synthesized at the Bayerisches Geoinstitut, Bayreuth (Germany) at intermediate conditions of $f(O_2)$, ~FMQ +1.1, where FMQ represents the log $f(O_2)$ value, in bars, at the fayalite – magnetite – quartz (FMQ) buffer. Two other series (AL and GB) were synthesized at the CRSCM (Orléans, France) at more oxidized (~FMQ + 2.4) and more reduced (~FMQ) conditions, respectively. Their H_2O contents range between 5.8 and 7.2 wt.% (Linnen *et al*. 1996), as determined from Karl Fisher titrations (Behrens 1995). The amounts of Sn(IV) were predicted on the basis of measurements of cassiterite solubility, in turn based on electron-microprobe measurements (Linnen *et al*. 1996).

TABLE 1. REDOX INFORMATION FOR THE MODEL COMPOUNDS OF TIN STUDIED

Models	E_0 energy (eV) *	Tin redox
Sn(0)	29199.5	0
Sn(II)O	29201.2	2
$Sn(II)Cl_2$	29201.1	2
$Sn(IV)O_2$ cassiterite, Bolivia	29204.2	4
$Ca_2Sn(IV)Al_2Si_6O_{18}(OH)_2(H_2O)_2$ eakerite, Foote mine, North Carolina, USA	29204.4	4
$Sn(IV)SrO_3$	29204.0	4
$CdSn(IV)(OH)_6$	29204.1	4
$CaSn(IV)O_3$	29204.1	4

* "half-way" of the edge method.

X-ray absorption fine structure

X-ray absorption fine structure (XAFS) spectra were collected (293 K) at the Stanford Synchrotron Radiation Laboratory on wiggler beamline 4–1 using a Si(220) double-crystal monochromator and a Stern–Heald-type fluorescence detector (Lytle *et al*. 1984). The tin *K*-edge is located at very high energy (29 keV) for most current synchrotron facilities. Therefore, the amount of beam available at these energies is generally limited, resulting in more difficult experimental conditions, namely much noisier spectra (the use of the tin L_{III} edge at 4 keV has other constraints and was not analyzed, as explained in the Introduction). In order to increase the signal:noise ratio, the fluorescence detector was filled with Xe gas, and slits before and after the monochromator were left relatively open (1 mm vertical aperture). The XANES and EXAFS data were reduced as previously reported (see Farges *et al*. 2006) using the XAFS package (Winterer 1997), following the recommendations of the International XAFS Society (IXS) Standards and Criteria (Sayers 2000).

XANES. All spectra were normalized for absorbance following standard methods (before the edge: $\mu m \rightarrow 0$, and after the edge: $\mu m \rightarrow 1$). All spectra were also checked for their energy calibration using a metallic tin foil (second transmission mode). To measure redox states, the "E_0" energy for each compound (references and glasses) was measured "half-way" in the absorption edge (*i.e*., at the energy where the normalized absorption coefficient is 1/2). The E_0 values and their standard deviations (computed on the basis of E_0 measurements performed on 3 to 10 replicate XANES measurements) are listed in Table 1. The standard deviations are relatively high, but this is expected given the intrinsic low resolution of the experiments and the need to obtain a high enough signal:noise ratio in the spectra, particularly for the glasses with dilute concentrations of Sn.

EXAFS. The eakerite model compound was used to extract amplitude and phases for the Sn–O and Sn–Si pairs in all Sn-bearing glasses. The EXAFS model of the Sn(II)–O pair in romarchite was tested using the functions extracted from eakerite to test the transferability from Sn(II) to Sn(IV). The model resulted in 5.5(2) atoms of oxygen at 2.210(3) Å instead of four atoms of oxygen at 2.224 Å (Pannetier & Denes 1980). Therefore, the use of the amplitude and phase-shift functions for the Sn(IV)–O pair results in an overestimation of

~1/2 of the actual number of Sn(II)–O neighbors. This is because the Sn(II)–O bonds are more ionic than Sn(IV)–O bonds, related to the relatively high Debye temperature of Sn(II) oxides (~280 K; Giefers & Wortmann 2002). Consequently, the glasses with the highest proportions of Sn(II) show much noisier spectra than for Sn(IV)-bearing glasses with the same concentration of tin. However, the temperature-induced anharmonicity remains small enough at room temperature (~10^{-3} $Å^{-3}$ for SnO; Giefers & Wortmann 2002) such that a harmonic approximation remains good enough to model the EXAFS signals below ~400 K. Indeed, the average Sn(II)–O distance at 290 K in romarchite was accurately estimated to within ±0.01 Å using the harmonic approximation. It is thus possible to use the harmonic approximation, which minimizes the number of parameters required to model the EXAFS spectra for the glasses. Where present (AL, SQ, GB ASI 0.6 compositions), silicon next-nearest neighbors were also included in the model as a second shell. For the SQ ASI 1.0 glass, we could not obtain a robust model of the EXAFS, which is due to the greater amount of noise in the data (related to the very low tin concentration of that glass, 1000 ppm, as well as the relatively high amount of the more ionic Sn(II).

Results

Models

Figure 1a shows the normalized XANES spectra collected for a variety of tin-bearing phases. These model compounds have a tin redox states of 0 (metal), +2 (romarchite and $SnCl_2$) or +4 (cassiterite, Sn-bearing perovskite and eakerite). Despite the relatively large broadening of the tin *K*-edge (~6 eV, convoluted from core-hole lifetime and experimental resolution; Krause & Oliver 1979), the tin *K*-edge shifts by ~5 eV from the metallic state (E_0 = 29199.5 eV) to the tetravalent state (E_0 = 29204.5 eV in eakerite; Fig. 1b). In agreement with previous studies (such as that of Mukerjee & McBreen 1999), the shift in the XANES edge position between Sn(II) and Sn(IV) is nearly twice that between Sn(0) and Sn(II) (Fig. 1b, Table 1). The *K*-edge EXAFS spectra of tin and their Fourier transforms (FT) are presented for the models in Figures 2a and b, respectively. The peak assignments on the FTs shown in Figure 2b is based on analysis of the crystal structures for these compounds. Among others, cassiterite can be detected by the presence of relatively large Sn–Sn contributions near 2.9 and 3.7 Å on the FT (on which distances are not corrected for the back-scattering phase-shift). These contributions correspond to the Sn–Sn pairs at 3.18 and 3.70 Å in cassiterite (Seki *et al.* 1984). The Sn–Si contributions near 3 Å on the FT of eakerite (3.31–3.33 Å if corrected for phase-shifts; Kossiakoff & Leavens 1976) can easily be distinguished from those of Sn–Sn contributions (as in cassiterite) because of the large differences in back-scattering amplitude and phase shifts between silicon and tin neighbors (as the appropriate back-scattering amplitude and phase shifts are required during the EXAFS modeling). This EXAFS and FT information for models can be used to detect in the glass the presence of Sn–Sn pairs and any nuclei (or partial dissolution) of SnO_2 at the ångström scale in the glasses. Because we never observed the next-nearest neighbors of tin in the 3–4 Å vicinity of the tin atom, we can confirm that no nucleation (or saturation) of cassiterite has occurred in a significant manner in any of the glasses studied.

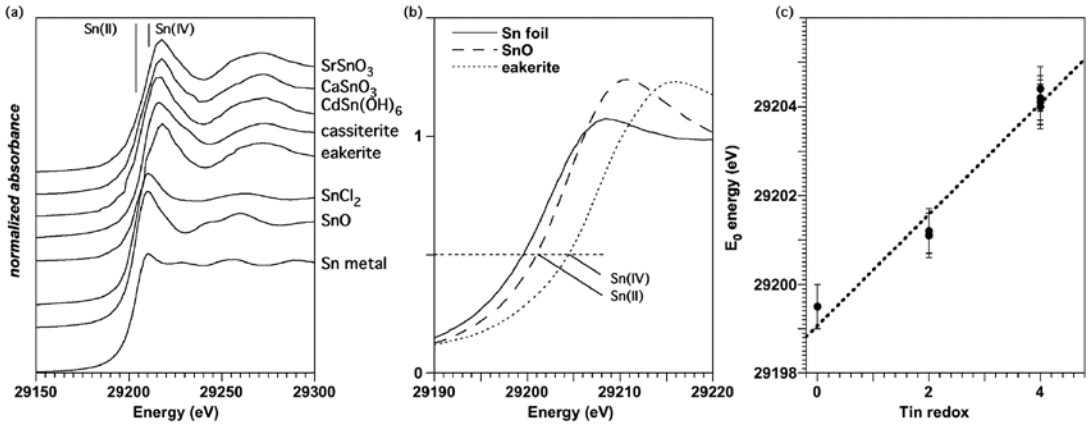

FIG. 1. (a) Normalized Sn K-edge XANES spectra for various model compounds of Sn(0), Sn(II) and Sn(IV). (b) Overlapped normalized XANES spectra for metallic tin, romarchite and eakerite, showing the shift in edge-energy position.

Silicate glasses: redox estimations

Figure 3a shows the normalized *K*-edge XANES spectra of tin collected for the three series of glasses, which show systematic shifts in energy position ("half-way" of the edge method; Fig. 3b) with glass composition. We emphasize that the edge crest (near 29215 eV) should not be used to monitor redox state, as this feature is also influenced by the local structure of tin (number of neighbors, distance to the absorbing tin atoms and various disorder terms). All ASI 0.6 glasses show dominant amounts of Sn(IV), whereas the *K*-edge XANES spectra of tin for the ASI 1.0 and ASI 1.2 compositions are significantly shifted toward lower energies, indicating the presence of Sn(II). Significant amounts of metallic tin were not found in any of the glasses, confirming the solubility models of Linnen *et al*. (1996), which did not require the presence of major amounts of metallic tin. In Table 2, we summarize the redox states of tin obtained for the glasses in this study, most of which compare well with the redox states that were estimated indirectly from measurements of cassiterite solubility (Linnen *et al*. 1996), particularly the peralkaline and peraluminous compositions (ASI 0.6 and 1.2, respectively). For instance, the estimated redox values from XANES data for the ASI 0.6 compositions range from 3.5 to 4.1 (±0.5), whereas the indirect estimates from solubility range from 3.0 to 3.9 (±0.3). In contrast, the ASI 1.2 compositions show large amounts of Sn(II). The estimated redox values from the XANES data for these compositions range from 1.7 to 2.1 (±0.5), whereas the indirect estimates from solubility range from 2.1 to 3.1 (±0.3).

However, larger discrepancies are found for the ASI 1.0 compositions, in which Sn(II) and Sn(IV) both are significant (according to the XANES). Figure 3b shows that the edge position for the AL ASI 1.0 glass

TABLE 2. REDOX INFORMATION FOR THE HYDROUS TIN-BEARING SILICATE GLASSES STUDIED

Glasses	chemical information		XANES information	
	SnO_2 (wt.%)*	Estimated average redox*	E_0 energy (eV)	Estimated average redox
Al ASI 0.6	1.0	3.9	29204.3	4.1
Al ASI 1.0	0.04	2.4	29203.2	3.3
Al ASI 1.2	0.05	3.1	29201.7	2.1
GB ASI 0.6	1.0	3.0	29203.6	3.6
GB ASI 1.0	0.6	2.4	29202.9	3.1
GB ASI 1.2	0.6	2.1	29201.2	1.7
SQ ASI 0.6	0.95	3.6	29203.5	3.5
SQ ASI 1.0	0.1	2.1	29202.8	3.0
SQ ASI 1.2	0.2	2.4	29201.1	1.7
reproducibility		0.3	*0.5*	*0.5*

* values from Linnen *et al.* (1996).

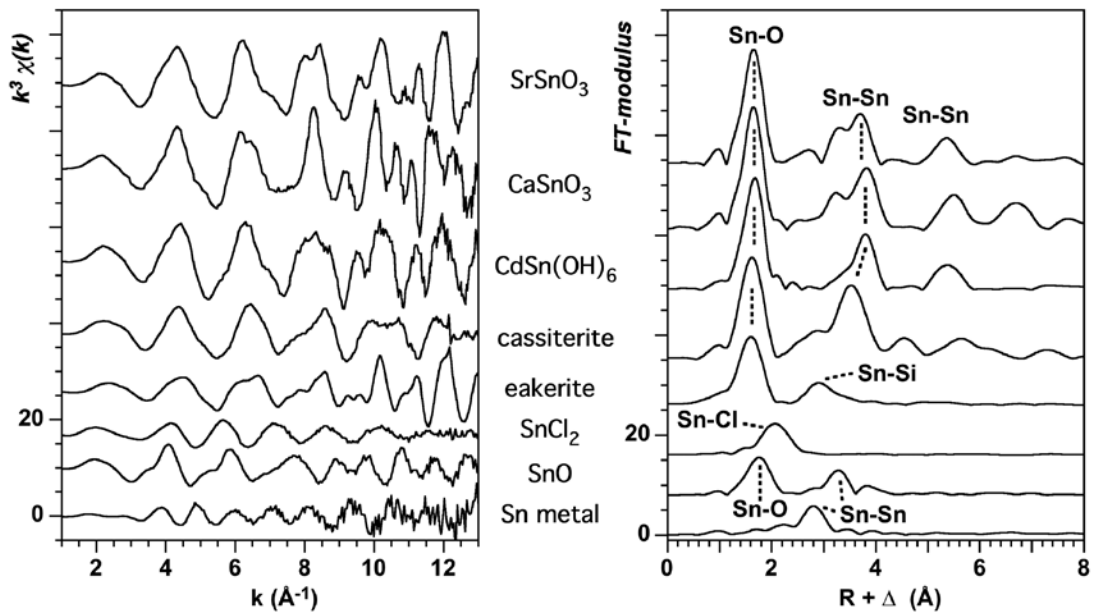

FIG. 2. Normalized EXAFS spectra (left) and their corresponding FTs (right) for the model compounds, showing the various pair of atoms and potential pairs with tin.

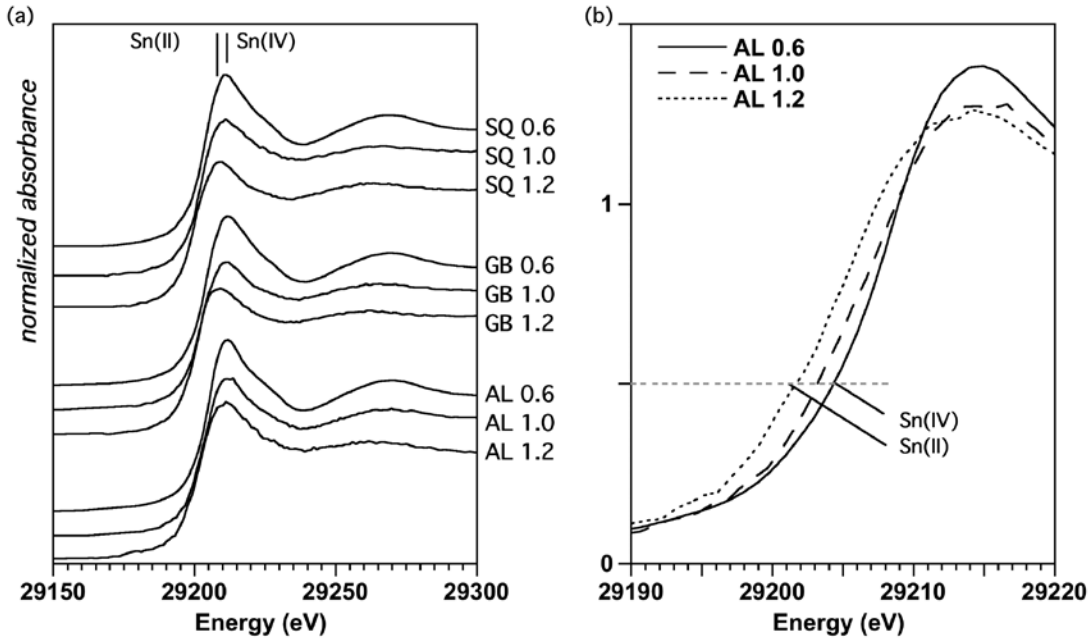

FIG. 3. (a) Normalized *K*-edge XANES spectra for tin for the glasses of this study. (b) Overlapped normalized XANES spectra for the three AL glasses (using the template of Fig. 1b), showing their shift in energy as a function of the redox state of Sn.

is not consistent with dominant amounts of Sn(II). The source of the disagreement is not clear to us, as it can be related to the solubility experiments or to the collection of XAFS data. It should be noted that the redox values estimated from solubility measurements are indirect, and are particularly susceptible to error at conditions where the redox state of tin varies. Also, a variety of solubility mechanisms at the ångström scale are possible (such as nanoscaled passivating environments, for which it is difficult to obtain evidence), and these mechanisms cannot be resolved with macroscopic information on solubility, even at the μm scale. On the other hand, information on the *K*-edge XANES edge position of tin is limited in accuracy by the relatively low-resolution conditions of the present XAFS experiments. For instance, the XANES position for the glass AL ASI 1.2 indicates dominant amounts of Sn(II). In contrast, the EXAFS and FT spectra for this last glass (Fig. 4) are consistent with an equal mixture of Sn(II) and Sn(IV), in agreement with the solubility measurements (estimated average redox of 3.1). In contrast, for the glass GB ASI 0.6, the EXAFS and FT spectra (Fig. 4) clearly indicate that tin is present dominantly as Sn(IV), in agreement with the XANES *K*-edge position. However, this information is in disagreement with solubility information (which suggests an average redox of 3.0). Therefore, in a number of cases, it is not easy to reconcile the redox state from the two sources of information.

Sn(IV) in glasses

Figures 4a and 4b show the normalized EXAFS spectra for the nine glasses of this study and their respective Fourier Transforms. The FTs for the peralkaline ASI 0.6 compositions (either GB, AL or SQ) are similar. They show two main contributions. The first contribution arises from oxygen first-neighbors (located near 1.6 Å on the FT). Non-linear models of the EXAFS spectra (Levenberg–Marquardt fitting method; see Fig. 5) suggests an average Sn–O distance of ~2.03(2) Å for these three glasses. This distance is typical of $Sn(IV)O_6$ moieties, as in the model compounds of Sn(IV) investigated, particularly eakerite. This average Sn–O distance in ASI 0.6 glasses is slightly lower than that found in cassiterite (<Sn–O> ~2.05 Å; Seki *et al.* 1984), Sr-bearing perovskite-group phases (Vallet-Regi *et al.* 1986) or sørensenite [$Na_4SnBe_2(Si_6O_{18})(H_2O)_2$; Maksimova 1973]. Also, this average Sn–O distance is much higher than that measured in pabstite [~ 2.00 Å; BaSn(Si3O9); Hawthorne (1987)]. No evidence for 4- or 5-coordinated Sn(IV) (as observed in K_2SnO_4; Gatehouse & Lloyd 1970) was found in these glasses. No short "tinyl" distance (~1.84–1.89 Å, within a five-coordinated square pyramid polyhedron) was found in

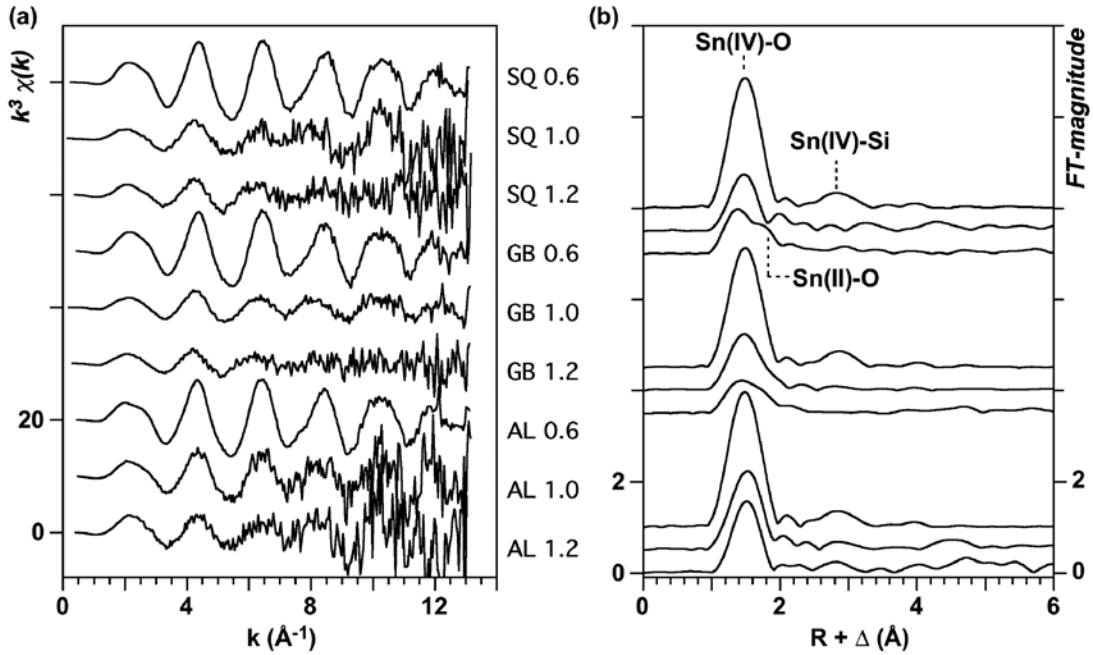

FIG. 4. Normalized EXAFS spectra (left) and their corresponding FTs (right) for the glasses of this study, showing the various pair of atoms and potential pairs, particularly Sn–O and Sn–Si pairs in the glasses containing dominantly Sn(IV). Note the higher signal:noise ratio in the glasses containing high amounts of Sn(II).

any of the glasses studied here [as observed for Ti(IV) in glasses and melts; Farges *et al*. 1996a, b].

In the peralkaline glasses (all of the ASI 0.6 samples), a second contribution to the tin *K*-edge EXAFS (located near 3 Å on the FT, uncorrected for phase shifts) arises from next-nearest neighbors with a relatively low Z-number, such as the network formers Si or Al. Network modifiers (such as alkali and alkaline earth elements) make bonds that are too ionic to be well detected (promoting both static and thermal disorder). *Ab initio* EXAFS calculations (using the FEFF8.2 package; Ankudinov *et al*. 1998) for eakerite and sørensenite confirm that Sn–Ca,Na contributions are much less detectable by EXAFS spectroscopy, in contrast to the Sn–Si contributions. Finally, the presence of tin next-nearest neighbors is excluded, because the shape of the back-scattering amplitude function for these neighbors is not compatible with the presence of atoms with relatively high Z-number (such as tin). In fact, the EXAFS spectra for the three ASI 0.6 glasses, in which tin is dominantly Sn(IV), are very close to that for eakerite, making this model compound particularly well suited to describe the local structure of Sn(IV) in glasses (compare both FT on Figs. 2 and 4). In eakerite, the SnO_6 units connect to network forming Si atoms through cornerr occupied by non-bridging atoms

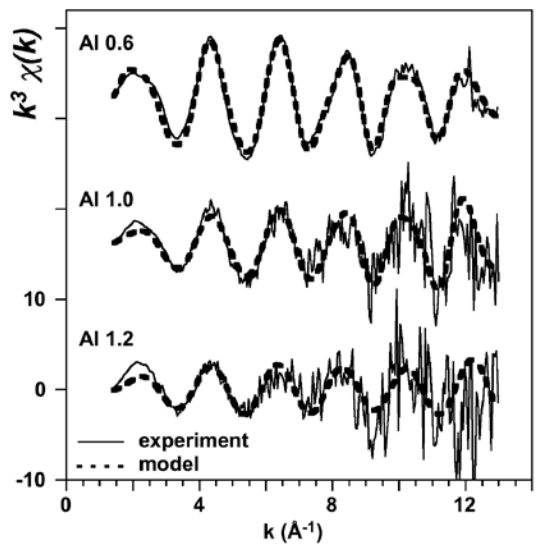

FIG. 5. Example of models (dotted lines) of the EXAFS spectra (solid lines) for the glasses of the series Al 1.0 and Al 1.2.

oxygens (NBO; resulting in Sn–O–Si angles ~107-132°; Kossiakoff & Leavens 1976). The SnO_6–SiO_4 units are then charge-compensated by network modifiers (alkalis, alkaline earths).

Sn(II): a very different speciation than Sn(IV) in glasses

In the metaluminous (ASI 1.0) and peraluminous glasses (ASI 1.2), the EXAFS spectra are noisier because of the relatively low contents of tin in these glasses (necessary to avoid saturation in cassiterite), but also because of the presence of Sn(II), evident from the comparison of cassiterite and romarchite, as discussed above. In addition, in the glasses that contain the most reduced tin (SQ ASI 1.2 and GB ASI 1.2), the presence of Sn(II) is detected as a peak on the FT that is related to a Sn–O pair near 1.8 Å (uncorrected phase-shift position). These longer Sn–O distances (~2.01–2.09 Å if corrected for Sn–O phase-shifts: see Table 3) are due to the much larger ionic radius of Sn(II) as compared to Sn(IV) (0.93 and 0.69 Å, respectively; Shannon & Prewitt 1969). Furthermore, because of this larger ionic radius, Sn(II) also forms highly asymmetric (anharmonic) environments (as in romarchite or thoreaulite). Consequently, the magnitude of the Sn(II)–O peak remains much lower than that for Sn(IV)–O (even in the most reduced glasses) because of the much lower EXAFS amplitude for Sn(II). Consequently, on the FT, the contribution for Sn(II) appears as a shoulder located on the high-distance side of the peak for Sn(IV). This also suggests that Sn(IV) still occurs in the most peraluminous glasses of this study (~25 atom % of the total tin). The average redox of tin in the present "ASI 1.0" glasses is therefore ~2.5, which is consistent with the redox information obtained from both the XANES and the information on cassiterite solubility (Linnen *et al.* 1996; Table 2). Finally, no evidence for next-nearest neighbors is observed around Sn(II), as a consequence of the high radial disorder among these next-nearest neighbors.

TABLE 3. EXAFS PARAMETERS FOR THE TIN-BEARING HYDROUS SILICATE GLASSES STUDIED

Glass		Shell	N	R (Å)	σ^2 (Å^2)	ΔE_0 (eV)	χ^2
Al	ASI 0.6	O	6.9(5)	2.035(5)	$1.0(5) \times 10^{-4}$	-1(2)	0.96
		Si	3.2(3)	3.34(2)	$4(3) \times 10^{-3}$	1(2)	
Al	ASI 1.0	O	5.9(5)	2.035(5)	$1(5) \times 10^{-4}$	-1(2)	3.19
		Si	1(1)	3.3(1)	$5(2) \times 10^{-3}$	0(2)	
Al	ASI 1.2	O	1.4(7)	2.01(1)	$7(1) \times 10^{-3}$	2(2)	5.12
		Si [1]	*2(1)*	*3.2(3)*	*3(3) × 10^{-3}*	*0(1)*	
GB	ASI 0.6	O	6.8(6)	2.034(5)	$0.8(6) \times 10^{-4}$	0.1(5)	1.12
		Si	4.1(2)	3.35(2)	$0.1(1) \times 10^{-3}$	1.7(3)	
GB	ASI 1.0	O	3.0(7)	2.047(5)	$1(1) \times 10^{-3}$	-1.5(2)	1.28
		Si	2(4)	3.3(1)	$3(1) \times 10^{-3}$	0(9)	
GB	ASI 1.2	O	4(2)	2.09(5)	$11(9) \times 10^{-2}$	0(3)	1.80
		Si [1]	*1(5)*	*3.2(2)*	*4(3) × 10^{-3}*	*0(1)*	
SQ	ASI 0.6	O	6.8(5)	2.029(4)	$0(5) \times 10^{-4}$	-0.1(4)	1.09
		Si	3.3(4)	3.34(2)	$4(3) \times 10^{-3}$	2(2)	
SQ	ASI 1.2	O	5(2)	2.08(5)	$13(1) \times 10^{-2}$	0(3)	1.98

[1] the parameters for this shell are less accurate: both the goodness of the fit and the χ^2 are lower and higher, respectively. χ^2 is defined as $\frac{n}{\upsilon \cdot M} \sum_{i=1,M} \frac{\left(d_i^2 - f_i^2\right)}{e_i^2}$, in which n is the number of independent data, υ, the degrees of freedom for the p free fit parameters, M is the number of data fitted, d_i is the data vector ("experiment"), f_i is the fit function vector ("model") and e_i is the absolute error of data vector ("standard deviation"). The goodness of fit is defined here a "degrees of freedom adjusted R^2", which equals to $1 - \sum_{i=1}^{n-1} w_i (d_i - \bar{f}_i)^2 / \sum_{i=1}^{\upsilon} w_i (d_i - \bar{f}_i)^2$.

Fits are relative to eakerite for Sn-O and Sn-Si pairs (6 atoms at 2.03 and 3.34 Å, respectively; Kossiakoff & Leavens (1976)

EXAFS for glass SQ ASI 1.0 could not be modeled

DISCUSSION

Eakerite and the importance of alkali- and alkaline-earth-bearing stannosilicates

On the basis of the present XAFS information, eakerite, although rare in nature, is an excellent structural model for Sn(IV) in glasses. Bond-valence calculations for octahedrally coordinated Sn(IV) (Pauling 1929) suggest that the average Sn(IV)–O bond valence is relatively high (= IV/6 valence units, *vu*). This bond valence is markedly different than that for Ti(IV) (average of 0.95 *vu*), which acts dominantly as a network former through titanyl moieties (Farges *et al.* 1996b). Also, because of this high average Sn(IV)–O bond valence, the thermal expansion of the Sn(IV)–O bond is predicted to be relatively low (below 10^5 K^{-1}; Farges & Brown 1996). Consequently, Sn(IV) will not be highly sensitive to thermal expansion (and compression), except at extreme conditions (*e.g.*, well above 2000 K, 100 kbar). Therefore, it is reasonable that the speciation information obtained for Sn(IV) in silicate glasses below 2000 K can be extrapolated to densified melts of geochemical interest, as shown for Zr (Brown *et al.* 1995, Farges *et al.* 2005).

The study of adequate model compounds such as eakerite also provides useful information on the connectivity of tetravalent tin to the framework of tetrahedra. From the Sn–O and Sn–Si distances (averages near 2.03 and 3.3 Å, respectively: Table 3) and the Si–O distances known in glasses (average ~1.62 Å; Brown *et al.* 1995), one can calculate an average Sn–O–Si angle of 140 (±10)° in glasses (maximum 132° in eakerite: Kossiakoff & Leavens 1976). This relatively large Sn–O–Si angle is typical of corner-shared SnO_6^{8-} and SiO_4^{4-} moieties (as in quartz). This is also consistent with Pauling's third rule (Pauling 1929), which states that highly charged cations preferentially share corners in cases where their ionic radius is relatively small (as for Si). In eakerite, SnO_6 and CaO_8 polyhedra share

edges (<Sn–O–Ca> = 104°; Kossiakoff & Leavens 1976), again in agreement with Pauling's third rule (as alkalis, by contrast, are predicted to share edges because of their lower charge and high ionic radii). The same topology was observed in all naturally occurring stannosilicates, including malayaite, pabstite, vistepite, tumchaite, sørensenite or brannockite, in which a variety of network modifiers are encountered (Na, K, Ca, Mn).

Structural role of Sn(IV)

Naski & Hess (1985) and Ellison *et al*. (1998) proposed that Sn(IV) forms "K_2SnO_4 complexes" in dry, peralkaline liquids at oxidized conditions. The concept of such "complexes" is inferred from information on saturation. However, these descriptions are inconsistent with the current framework of knowledge about the structure of oxide glasses and melts [see Mysen (1990) for a review]. A large number of spectroscopic and scattering data have established that silicate glasses and melts comprise a coherent aperiodic structure, consisting of network formers and modifiers connected through bridging and non-bridging oxygen atoms (the "tetrahedral network model"). Only a few cations, such as Mo(VI) or W(VI), are truly able to form "complexes" because of their very high bond-valences (~1.5 *vu*) in oxide glasses and melts (see below). Tin "complexes" cannot exist because the average Sn–O bond valence is well below 1 *vu*, as described above.

Within the "tetrahedral network model", the oxygen atoms connecting tin to the framework of tetrahedra (mostly SiO_4 and AlO_4 units) cannot bond to more than one silicon atom; otherwise these atoms of oxygen would be severely overbonded. Also, these atoms of oxygen are unlikely to bond only to network modifiers (NM) because Sn–Si pairs are detected by the EXAFS spectra for Sn(IV)-bearing glasses. Consequently, these connecting atoms of oxygen must connect to one tin, one silicon and one or two network modifier(s) so that the sum of bond valences around these atoms of oxygen equals 2 (see Fig. 6 in Farges *et al*. 1991). The connecting atoms of oxygen between tin and silicon are consequently non-bridging oxygen atoms (NBO). In eakerite, for instance, these connecting oxygen atoms, O_1, O_4 and O_6, according to Kossiakoff & Leavens (1976), are all three-coordinated with silicon at 1.60 Å, tin at 2.06 Å and calcium at 2.40 Å (Fig. 6). Similarly, three-coordinated NBO atoms are observed in structures containing divalent cations for charge compensation of SnO_6 units, such as malayaite ($CaSnSiO_5$; Eremin *et al*. 2002), pabstite [$Ba(Sn,Ti)Si_3O_9$; Hawthorne (1987), or vistepite [$Mn_4SnB_2(SiO_4)_4(OH)_2$; Hybler *et al*. 1997]. These three-coordinated NBO atoms are also observed where smaller alkalis are present, such as in brannockite ($KSn_2Li_3Si_{12}O_{30}$; Armbruster & Oberhänsli 1988) or in hydrous structures [as in tumchaite, $Na_2(Zr_{0.8}Sn_{0.2})Si_4O_{11}(H_2O)_2$, Subbotin *et al*. 2000]. In contrast, where the charge-compensating alkalis have a smaller ionic radius (Na instead of Ca or K), their coordination tends to be lower [see Brown *et al*. 1995 for a review], and the resulting bond-valence is higher. The efficiency of these charge-compensating cations to compensate the central highly charged cation is, then, increased. Consequently, two of these weakly bonded cations are required around the connecting NBO, as for atoms of oxygen O_3 in sørensenite [$Na_4SnBe_2(Si_3O_9)_2(H_2O)_2$; Metcalf Johansen & Gronbaek Hazell 1976]. Thus, the application of Pauling's second rule to our ASI 0.6 glasses requires that the oxygen first neighbors around

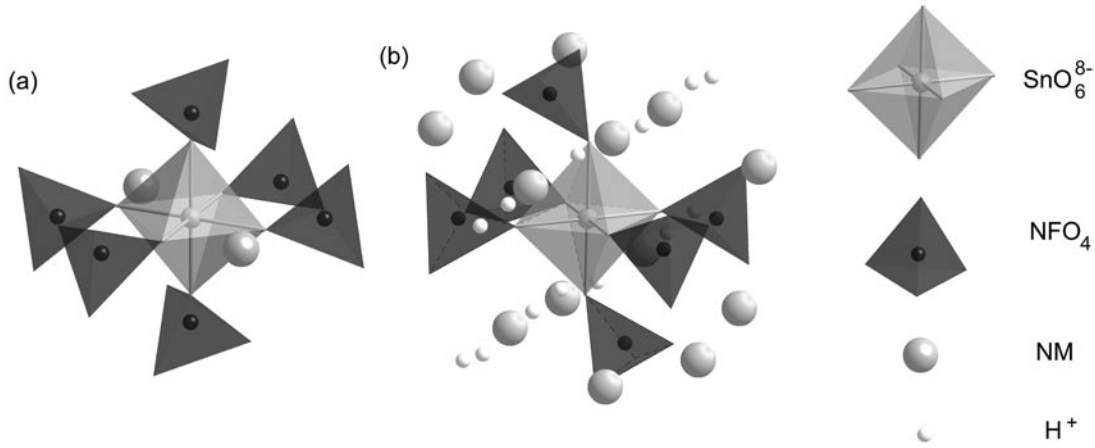

FIG. 6. Models of structure around a SnO_6^{8-} moiety: (a) local structure as in eakerite, showing 3-coordinated atoms of oxygen around Sn(IV), which are charge-compensated by tetrahedrally coordinated network-formers (NF) and network-modifiers (NM). (b) Local structure as in tumchaite, showing the distant protons (H^+) that cannot bond directly to the SnO_6^{8-} moiety.

Sn(IV) be non-bridging, as they must connect to one network former (NF = Si or Al) and to two network modifiers (NM = Na or K), as shown on Figure 6 (the same topology was found around Zr in glasses; Farges *et al.* 1991). However, these Na,K network modifiers form ionic bonds, such that they cannot easily be detected by XAFS methods, particularly in aperiodic structures like glasses or melts. Pauling's second rule, in addition, suggests that Sn(IV) polyhedra must share edges with network modifiers, including in the present glasses. Because of its bonding properties, Sn(IV) cannot be a network former because of its average bond-valence to NBO (~0.67 *vu*), at variance with the findings of Linnen *et al.* (1996). Consequently, the observed coupling between Sn(IV) and network formers, and its anti-coupling with network modifiers (Linnen *et al.* 1996), reflect the bonding requirements of Sn(IV), which must connect to non-bridging atoms of oxygen.

Influence of H_2O: no evidence for "complexes"

Examination of the crystal chemistry of Sn(IV) also suggests that hydroxyl groups cannot bond directly to Sn(IV) in the vicinity of silicon next-nearest neighbors. If they could exist, such oxygen atoms would be three-coordinated, and bonded to one tin, one silicon and one hydrogen (the hydroxyl bond). In sørensenite, $Na_4SnBe_2Si_6O_{18}$•$2H_2O$ (Metcalf Johansen & Gronbaek Hazell 1976) or tumchaite, $Na_2(Zr,Sn)Si_4O_{11}$•$2H_2O$ (Subbotin *et al.* 2000), protons are located at 3.1–3.2 Å from the central tin atom (Fig. 6), but belong to more distant hydroxyl groups (in which oxygen atoms are located between 3.9 and 4.2 Å from the central Sn). Thus, such protons are not bonded to any tin. Again, Pauling's second rule provides a rationale for the lack of bonding of protons to the SnO_6^{8-} units. Hydroxyl groups provide ~0.7–0.8 valence units (Brown 1992), which is too high with respect to that for Sn–O (~0.7 *vu*) or for Si–O (~1.0 *vu*). Otherwise, the connecting three-coordinated oxygen would be overbonded by 0.7 + 1.0 + 0.7 – 2 = 0.4 *vu*. Consequently, the presence of SnO_6^{8-} units, together with Sn–Si pairs in the EXAFS of the ASI 0.6 glasses, does not favor the "complexation" of tin by hydroxyl groups or H_2O molecules in these samples.

Structural relations to solubility

In peralkaline compositions, there are enough network modifiers to charge-compensate Sn(IV), so that its solubility is greater, as reported by Hess (1991). The solubility of tin is enhanced, as a result of depolymerization, in compositions with greater concentrations of NBO atoms, *i.e.*, with increasing peralkalinity or in the presence of depolymerizing volatiles (such as H_2O and fluorine). If the melt is peraluminous, there is a shortage of NBO atoms to which Sn(IV) must bond (alternatively, tin can bond to aluminum triclusters to adapt to this shortage of NBO atoms). Consequently, Sn(IV) is expelled from the silicate melt and precipitates as cassiterite (SnO_2 saturation). Linnen *et al.* (1996) observed that peraluminosity favors Sn(II) at the expense of Sn(IV) in H_2O-saturated ASI glasses. Therefore, there is good agreement between the data on cassiterite solubility and the findings on speciation (Linnen *et al.* 1995, 1996, Linnen 2005).

Ellison *et al.* (1998) proposed that the solubility mechanisms for tin are similar to those for titanium. For glass and melts with high solubilities of titanium (*e.g.*, peralkaline melts), these authors reported that the coordination of titanium is 4 (*versus* 6 in metaluminous melts). Raman spectroscopy experiments have confirmed that four-coordinated titanium is actually present in most silicate glasses (Henderson & Fleet 1995, Reynard & Webb 1998) and, accordingly, titanium *K*-edge XANES spectroscopy indicates that 4-coordinated Ti is the dominant coordination in nearly fully polymerized compositions (such as in the ASI compositions of this study), *i.e.*, where NBO atoms are lacking in the melt (Farges *et al.* 1996b). No evidence for four-coordinated Sn(IV) was detected in any of the glasses studied, even in the most strongly peralkaline compositions. Consequently, tin and titanium seem to occupy very different structural positions in silicate glasses (and most likely in melts because of the high bond valence of Sn(IV)–O bonds). However, both cations form relatively rigid bonds to oxygen atoms, both requiring a number of non-bridging oxygen atoms with which to bond. Therefore, at a macroscopic scale, both tetravalent cations will be more soluble in NBO-rich compositions. Also, Ti and Sn would saturate in their respective oxide component (cassiterite and rutile) where NBO atoms are lacking, despite the fact that they occupy significantly different structural positions in the glass network.

Structural role of Sn(II)

Because of its higher ionicity and ionic radius, Sn(II) is expected to behave differently from Sn(IV). This is related to the higher ionicity of the Sn(II)–O bonds, as observed for example in thoreaulite ($SnTa_2O_6$; Maksimova *et al.* 1975). In this compound, Sn(II) is 8-coordinated and forms relatively ionic bonds (their bond valence is ~0.25 *vu*). In addition to thermal disorder (related to ionicity), a highly anharmonic radial-distribution function is observed for Sn–O in thoreaulite: the first neighbors around Sn are split between two shells containing five and three atoms of oxygen, centered at 2.16 and 2.43 Å, respectively. If corrected for back-scattering phase-shift, the (R + Δ) position for the Sn(II)–O peak observed on the FT for the reduced glasses of this study suggests a Sn(II)–O distance of ~2.2 Å, similar to the first set of Sn–O distances in thoreaulite. It is possible that a second set of Sn(II)–O distances (occurring at much greater distances) is present in the glasses,

but the intrinsic noise of the spectra [where Sn(II) dominates] hides this structural information.

Consequently, Sn(II) behaves more like a highly efficient network modifier, owing to its larger ionic radius and lower charge, promoting highly ionic bonds, high coordination and therefore, highly anharmonic environments. From the presence of ionic bonds around Sn(II), this ion is predicted to be much more sensitive than Sn(IV) to thermal expansion or melting (Brown *et al*. 1995). Thus, like other weakly bonded transition elements, Sn(II) should reduce its coordination in melts (*i.e*., 5, 6-coordinated, for instance). Therefore, Sn(II) behaves more like an efficient network modifier in silicate melts, like Pb^{2+} or Na^{+}. Consequently, divalent tin must also be sensitive to the presence of aluminum, as both cations can efficiently charge-compensate any non-bridging oxygen atom (Bhalla *et al*. 2005). In contrast, the influence of melt polymerization induced by fluorine on Sn(II) speciation must be less stringent because of the formation of Na–Si–F subnetworks in the melt (Zeng & Stebbins 2000). This is because Sn(II) makes bonds that are too strong for these Na–Si–F subnetworks; charge-compensating substitution of cations in such subnetworks requires ~0.1 *vu* for the 4-, 5- or 6-coordinated Si–F bondings (see Liu & Nekvasil 2002), but ~0.25 *vu* are provided by divalent tin. Bond-valence models for Sn(II) explain a number of other macroscopic observations. For example, the diffusivity of Sn(II) must be higher than that for Sn(IV) in such melts owing to lower bond-valence for Sn(II) as compared to Sn(IV). This is in agreement with Linnen *et al*. (1996), who also inferred that the coordination of tin in reduced (*i.e*., FMQ + 1) peraluminous melts [*i.e*., Sn(II)-rich] is greater than in peralkaline melts [in which Sn(IV) dominates].

Geochemical implications

Our study shows that Sn(IV) and Sn(II) differ significantly in the nature of their bonds to oxygen atoms (relatively more covalent and more ionic, respectively). To our knowledge, tin is probably the cation (together with lead) for which redox most affects its bonding requirements in silicate glasses and melts (much more than for ferrous and ferric iron, for instance). As compared to Sn(IV), Sn(II) must partition more favorably into NBO-rich melts (such as alkaline or hydrous melts) than into BO-rich melts (such as peraluminous or anhydrous melts). This could explain the formation of minerals of Sn(II), such as thoreaulite, in some rare late-stage depolymerized magmas and magmatic-hydrothermal fluids at the expense of cassiterite, these fluids also being sensitive to halogen (F and Cl) "complexation", as suggested by Keppler & Wyllie (1991), but observed only recently by Sherman *et al*. (2000). A similar phenomenon is observed for titanium and zirconium: their speciation in the "melt" is close to that of late-crystallizing alkali and alkaline-earth zirconosilicates and titanosilicates (such as catapleiite and fresnoite), whereas zircon and rutile (*i.e*., alkali- and alkaline-earth-free and highly depolymerized) are the common forms of Zr and Ti that nucleate from most melts (Farges *et al*. 1991, 1996a). In contrast, the addition of fluorine is predicted to produce the required non-bridging oxygen (as in hydrous metaluminous and peralkaline melts) and enhance mostly the solubility of tetravalent tin (Pichavant *et al*. 1987, Bhalla *et al*. 2005).

In contrast, in more oxidized granitic melts, Sn(IV) is present, but because it requires NBO that are lacking in these compositions, tin must be expelled from the framework of tetrahedra of the melt structure. Thus, cassiterite will precipitate from the late-stage residual melts (Linnen 2005). Finally, tin solubility is enhanced in peralkaline melts because of the availability of NBO to which tin must bond. This molecular mechanism corresponds to what Taylor (1979) reported about the solubility of tin as being controlled by the "melt basicity" through the activity of "free oxygen atoms". We need to restate this last conclusion, as free oxygen atoms do not exist in oxide melts [see Brown *et al*. (1995) and numerous molecular dynamics and ^{17}O NMR studies). Thus, in other words, Taylor's (1979) observations are consistent with an excess of NBO in peralkaline melts. Similarly, under hydrothermal conditions, Sn(IV) has been found to be more transportable by volatile complexation than previously thought (Sherman *et al*. 2000). Also, these authors showed that $Sn(IV)Cl_6^{2-}$ complexes precipitate as SnO_2 as both the concentration of tin and temperature of the sample increase. This behavior is consistent with the bond-valence models of Sn(IV) described above.

Comparison with related metals in silicate glasses: molybdenum, tungsten and tantalum

Molybdenum and tungsten. A variety of highly polymerized glasses (rhyolitic) were synthesized in air and doped with 300–1000 ppm molybdenum, tungsten and tantalum (Fig. 7). Synthesis and data-collection information for the molybdenum-bearing glasses are presented elsewhere (Farges *et al*. 2006). They were prepared under moderately oxidizing conditions (~NNO buffer). The tungsten-bearing glasses were synthesized in air. The tantalum-bearing glasses were prepared by one of us (R.L.L.) at Bayreuth under the same conditions as reported by Piilonen *et al*. (2005, 2006) for niobium-bearing glasses. The EXAFS for tungsten (as well as tantalum) could only be collected for a few model and glass samples, given the low intensity of their L_{III} edge jump.

The Mo *K*-edge XANES information for model compounds and rhyolitic glasses containing 0.1 to 3 wt.% molybdenum (Fig. 7a) show a large pre-edge feature, typical of a tetrahedral symmetry around molybdenum (see Farges *et al*. 2006). This pre-edge

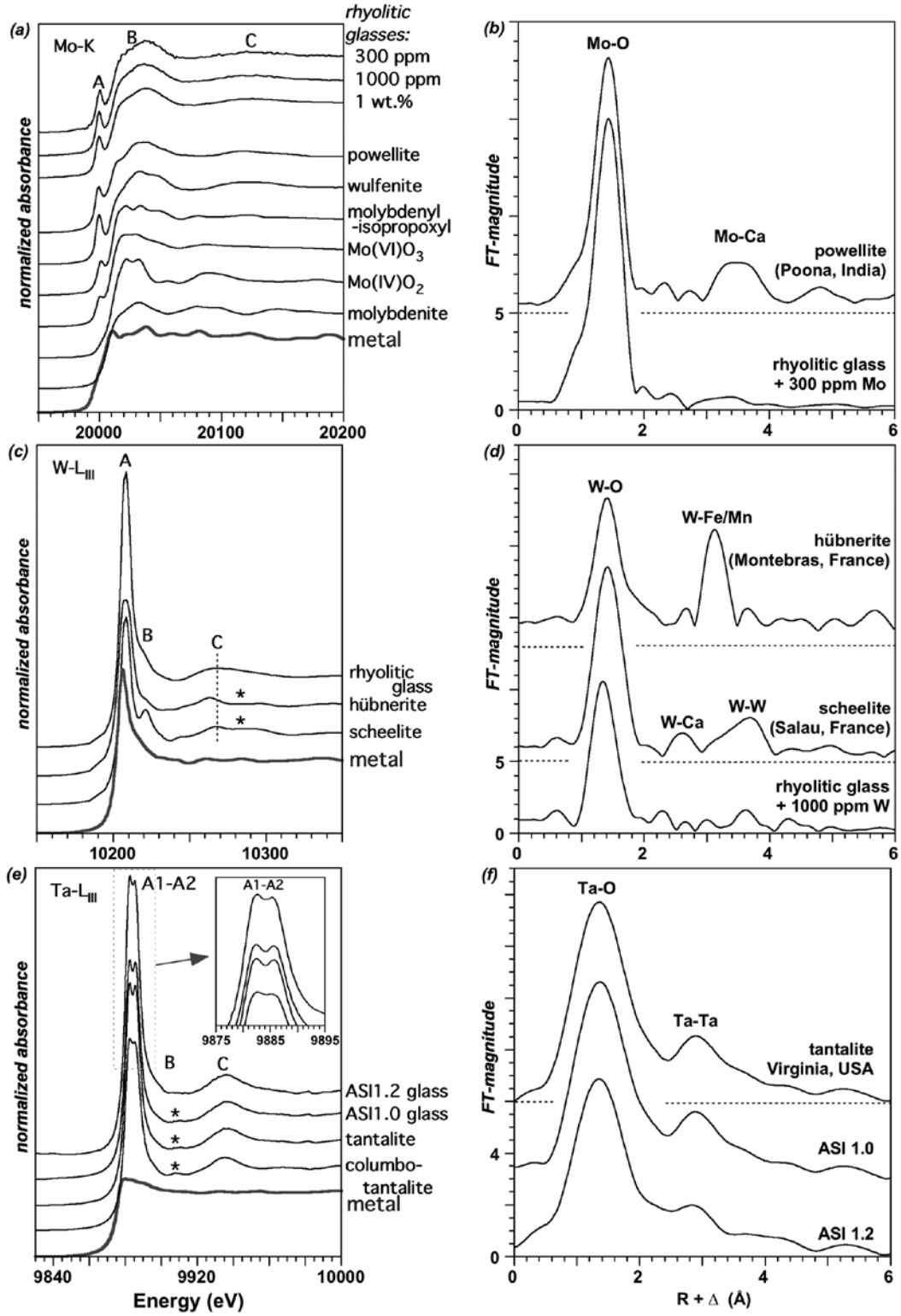
(a)
Mo-K
A
B
C
rhyolitic glasses:
300 ppm
1000 ppm
1 wt.%
powellite
wulfenite
molybdenyl -isopropoxyl
Mo(VI)O3
Mo(IV)O2
molybdenite
metal
normalized absorbance
20000
20100
20200
(b)
Mo-O
Mo-Ca
powellite (Poona, India)
rhyolitic glass + 300 ppm Mo
FT-magnitude
(c)
W-LIII
A
B
C
rhyolitic glass
hübnerite
scheelite
metal
10200
10300
(d)
W-O
W-Fe/Mn
hübnerite (Montebras, France)
W-Ca
W-W
scheelite (Salau, France)
rhyolitic glass + 1000 ppm W
(e)
Ta-LIII
A1-A2
ASI1.2 glass
ASI1.0 glass
tantalite
columbo-tantalite
metal
9840
9920
10000
Energy (eV)
(f)
Ta-O
Ta-Ta
tantalite Virginia, USA
ASI 1.0
ASI 1.2
R + Δ (Å)

is also present at relatively low fugacities of oxygen (FMQ–2). These glasses show a Mo–O peak on the FT located at 1.2 Å (1.8 Å if corrected for back-scattering phase-shifts; see Fig. 7b). This is consistent with the presence of molybdate moieties [$Mo(VI)O_4^{2-}$] in these rhyolitic glasses. Similar results are found for tungsten in rhyolitic glasses (1000 ppm). The XANES and EXAFS spectra for tungsten in these glasses (Figs. 7c and d, respectively) are closer to that for scheelite ($CaWO_4$) than that for hübnerite, $(Mn,Fe)WO_4$. This suggest the presence of tungstate moieities in the glasses [four-coordinated W(VI)] as in scheelite (Hazen *et al*. 1985) [W(VI) is six-coordinated in hübnerite]. This result is also in agreement with interpretations of the solubility of hübnerite and ferberite (Linnen 2005).

Molybdate and tungstate moieties are characterized by a very high average bond-valence (VI/4 = 1.5 valence units). Therefore, hexavalent molybdenum and tungsten can only be charge-compensated by network modifiers, which can easily provide the necessary 0.5 *vu* to charge-compensate the oxygen atoms in between Mo and W and the network modifiers (as in powellite, $CaMoO_4$; Hazen *et al*. 1985). In contrast, molybdate and tungstate moieties cannot bond to network formers (which provide 0.8–1.2 *vu*), as the connecting oxygen atoms would be severely overbonded (by 0.3–0.7 *vu*). This fact explains why hexavalent molybdenum and tungsten largely occur in non-silicate minerals in nature. Consequently, Mo(VI) and W(VI) are complex-formers in silicate glasses, and their polyhedra remain in the areas of the glass that are rich in network modifiers; thus they are not directly connected to the framework of tetrahedra.

Tantalum and niobium. Figure 7e shows the Ta L_{III}-edge XANES spectra for tantalum collected in a selection of ASI glasses. As for tungsten, few high-quality EXAFS spectra could be collected for tantalum because of the very low edge-jump at the L_{III} edge. However, the first EXAFS feature (feature C) and the edge position (feature A) are identical in the glasses and in columbite–tantalite model compounds, in which tantalum is 6-coordinated by oxygen atoms (Klein & Weitzel 1976). In the metaluminous glass (ASI 1.0), Ta–Ta pairs are observed in the Fourier Transform (near 2.8 Å on the FT, which is equivalent to a Ta–Ta distance of 3.2 Å; see Fig. 7e), indicating some saturation of the melt in tantalum. In addition, the well-defined Ta-L_{III} edge in ASI 1.2 (*i.e*., features A1–A2) suggests a well-ordered local structure in that glass, as compared to ASI 1.0, again confirming that this sample has ordered domains enriched in Ta (most likely an incomplete dissolution of Ta_2O_5). In contrast, the Ta–Ta contributions are much less intense in the peraluminous glass (ASI 1.2), indicating a better dissolution of Ta in that composition. The speciation information for Ta(V) in the latter glass is similar to that for Nb(IV) in a variety of dry and H_2O-saturated haplogranitic melts (Piilonen *et al*. 2002, 2006), which were interpreted to reflect the presence of NbO_6^{7-} units connected to the framework of tetrahedra (in agreement with a variety of Raman scattering and Nb_2O_5 solubility experiments).

From this set of information, only molybdenum and tungsten are (true) complex-formers that remain disconnected from the network of tetrahedra (making them easily extractable by fluids) under moderately reducing conditions. This property is principally due to their high bond-valence (~1.5 valence units). In contrast, Nb(V) and Ta(V) form much lower bond-valences (0.7–0.9 *vu*), making them weak network modifiers [like Zr or Sn(IV)]. These cations will, then, be much more sensitive to melt polymerization and alkalinity, as Sn(IV). Also, the excess of NBO atoms provided by H_2O in peralkaline melts should not influence the solubility of the accessory phases containing Nb, Ta, W and Mo as essential components (*e.g*., columbite–tantalite, ferberite–hübnerite solid-solutions), as there is a large excess of NBO atoms to which any of these cations and the network formers will bond. In contrast, aluminum and the high-field-strength element (HFSE) cations compete for NBO atoms in anhydrous metaluminous melts, so that NBO atoms resulting from the introduction of H_2O can strongly affect HFSE solubility (Linnen 2005).

However, under reducing conditions (~QFM buffer and below), the situation is dramatically different. Both Mo(V) and Mo(IV) appear at the expense of Mo(VI) (Farges *et al*. 2006). The average bond-valence of molybdenum falls drastically, to values close to 2/3, as Mo(IV) is found to be six-coordinated in highly reduced melts (~IW buffer and below; Farges *et al*. 2006). Most likely, tungsten will show the same behavior as molybdenum (but plausibly at different conditions of oxygen fugacity). As a consequence, in these reduced melts, molybdenum (and possibly tungsten) would behave like tetravalent tin. However, it is likely that under the reducing conditions required for Mo(IV) to form, tin is divalent (Linnen et al. 1996, this study). In this context, tin [as Sn(II)] is an "efficient" network modifier, a very unique case among HFSE elements. Thus, the mobility of divalent tin should be dramatically enhanced, also making it easily extractable by fluids. On the other hand, Mo(IV) should behave in a manner similar to Zr or Nb, unless sulfur is present, as it preferentially bonds with chalcophile elements such as molybdenum in S-bearing glasses (Farges *et al*. 2006). The consequence of an oxygen-to-sulfur change in ligands is the same as for the reduction of tin, *i.e*., a strong increase in

FIG. 7. Normalized XANES spectra (left) and FTs (right) of the EXAFS spectra (not shown) for a variety of models and glasses containing molybdenum (top figures), tungsten (middle figures) and tantalum (bottom figures).

ionicity and, thus, of mobility. This would enhance the extraction of tetravalent molybdenum sulfide species by fluids from coexisting melts, a feature that is not yet well recognized for tungsten (which is much less of a chalcophile element than molybdenum). Only niobium and tantalum are predicted to behave in a relatively comparable manner in reduced, volatile-bearing (H_2O, sulfur, fluorine, chlorine and CO_2), high-pressure oxide melt frameworks. Consequently, the chemical affinities for each of these metals are quite unique (Windy & Drake 2000), reinforcing the fact that the crystal chemistry for each of these rare metals in geochemically relevant melts is not easily predictable without a thorough investigation of their molecular-scale preferences in bonding in oxide melts.

Conclusions

In silicate glasses, Sn(IV) is present as eakerite-type moieties. Consequently, Sn(IV) behaves in a similar manner to Zr(IV), *i.e.*, it is highly dependent on the available non-bridging oxygen atoms to which Sn(IV) preferentially bonds. As a result, Sn(IV) is sensitive to melt depolymerization, alkalinity and fluid contents (all of which enhance the solubility of tetravalent tin). In contrast, Sn(II) is much more sensitive to temperature, and its structural environment is less well defined, owing to its higher ionicity. Thus Sn(II) is highly compatible with NBO-rich phases, such as magmatic-hydrothermal fluids or late peralkaline magmas. Tin in relatively reduced metaluminous to peraluminous melts (the melts from which tin granites crystallize) is dominantly present as Sn(II), in sharp contrast to the mineralogy of tin (for which cassiterite predominates). In addition to its large differences in behavior related to its two redox states, tin also behaves quite differently from Mo(VI) and W(VI) in silicate glasses, which form true complexes (molybdate and tungstate moieties, even at relatively low fugacities of oxygen), disconnected from the framework of tetrahedra. In contrast, Ta(V) and Nb(V) compounds are easily saturated in melts that lack network compensators, as with Sn(IV) or Ti(IV). This validates the information about these high-field-strength elements from thermochemistry (Hess 1991), although Sn, Nb, Ta and Ti have very different structural positions in silicate glasses and melts of geochemical interest. This information shows the variety of behaviors among related metals in magmatic systems; such variety is largely related to the differences in their bonding requirements, primarily controlled by their bond valence, which influences their ionicity and connectivity in glasses and in melts.

Acknowledgements

We thank the staff of SSRL for their help in data collection. The Stanford Synchrotron Radiation Laboratory is supported by DOE, Office of Basic Energy Sciences, and NIH, Biotechnology Resource Program, Division of Research Resources. Constructive, detailed comments by two anonymous referees, as well as guest editor I.M. Samson and R.F. Martin were greatly appreciated.

References

Armbruster, T. & Oberhänsli, R. (1988): Crystal chemistry of double-ring silicates: structures of sugilite and brannockite. *Am. Mineral.* **73**, 595-600.

Ankudinov, A.L., Ravel, B., Rehr, J.J. & Conradson, S.D. (1998): Real-space multiple scattering calculation and interpretation of x-ray absorption near-edge structure. *Phys. Rev.* **B 58**, 7565-7576.

Behrens, H. (1995): Determination of water solubilities in high-viscosity melts: an experimental study on $NaAlSi_3O_8$ and $KAlSi_3O_8$. *Eur. J. Mineral.* **7**, 905-920.

Bhalla, P., Holtz, F., Linnen, R.L. & Behrens, H. (2005): Solubility of cassiterite in evolved granitic melts; effect of T, fO_2 and additional volatiles. *Lithos* **80**, 387-400.

Brown, G.E., Jr., Farges, F. & Calas, G. (1995): X-ray scattering and X-ray spectroscopy studies of silicate melts. *In* Structure, Dynamics, and Properties of Silicate Melts (J.F. Stebbins, D.B. Dingwell & P.F. McMillan, eds.). *Rev. Mineral.* **32**, 317-408.

Brown, I.D. (1992): Chemical and steric constraints in inorganic solids. *Acta Crystallogr.* **B48**, 553-572.

Durasova, N.A., Kochnova, L.N., Ryabchikov, I.D. & Khramov, D.A. (1997): Tin-bearing aluminosilicate systems in high-temperature processes under variable redox conditions. *Geochem. Int.* **35**, 596-601.

Durasova, N.A., Ryabchikov, I.D. & Barsukov, V.L. (1986): The redox potential and the behavior of tin in magmatic systems. *Int. Geol. Rev.* **28**, 305-311.

Ellison, A.J., Hess, P.C. & Naski, G.C. (1998): Cassiterite solubility in high-silica K_2O–Al_2O_3–SiO_2 liquids. *J. Am. Ceram. Soc.* **81**, 3215-3220.

Eremin, N.N., Urusov, V.S., Rusakov, V.S. & Yakubovich, O.V. (2002): Precision X-ray diffraction and Mössbauer studies and computer simulation of the structure and properties of malayaite $CaSnOSiO_5$. *Kristallografiya* **47**, 825-833.

Eugster, H.P. (1985): Granites and hydrothermal ore deposits: a geochemical framework. *Mineral. Mag.* **49**, 7-23.

Farges, F. & Brown, G.E., Jr. (1996): An empirical model for the anharmonic analysis of high-temperature XAFS spectra of oxide compounds with applications to the coordination environment of Ni in Ni-olivine and Ni–Na-disilicate glass and melt. *Chem. Geol.* **127**, 253-268.

FARGES, F., BROWN, G.E., JR., NAVROTSKY, A., GAN, H. & REHR J.J. (1996a): Coordination chemistry of Ti(IV) in silicate glasses and melts. II. Glasses under ambient conditions. *Geochim. Cosmochim. Acta* **60**, 3039-3054.

FARGES, F., BROWN G.E., JR., NAVROTSKY, A., GAN, H. & REHR J.J. (1996b): Coordination chemistry of Ti(IV) in silicate glasses and melts. III. Glasses and melts between 293 and 1650 K. *Geochim. Cosmochim. Acta* **60**, 3055-3065.

FARGES, F., DJANARTHANY, S., DE WISPALAERE, S., MUNOZ, M., WILKE, M., BORCHERT, M., SCHMIDT, C., TROCELLIER, P., CRICHTON, W., SIMIONOVICI, A., PETIT, P.-E., MEZOUARD, M., ETCHEVERRY, M.-P. & PALLOT-FROSSARD I. (2005): Water in silicate glasses and melts of environmental interest: from volcanoes to cathedrals. *Phys. Chem. Glasses* (*in press*).

FARGES, F., PONADER, C.W. & BROWN, G.E., JR. (1991): Local environment around incompatible elements in silicate glass/melt systems. I. Zr at trace levels. *Geochim. Cosmochim. Acta* **55**, 1563-1574.

FARGES, F., SIEWERT, S., BROWN, G.E., JR., GUESDON, A. & MORIN, G. (2006): Structural environments of molybdenum in silicate glasses and melts. I. Influence of composition and oxygen fugacity on the local structure of molybdenum. *Can. Mineral.* **44**, 731-753.

GATEHOUSE, B.M. & LLOYD, D.J. (1970): The crystal structure of potassium metazirconate, K_2ZrO_3, and its tin analogue, K_2SnO_4 [erratum: K_2SnO_3]. *J. Solid State Chem.* **2**, 410-415.

GIEFERS, H. & WORTMANN, G. (2002): EXAFS study of SnO and SnO_2 between 22 K and 623 K. *Hasylab Activity Report* **2001**.

HAWTHORNE, F.C. (1987): The crystal chemistry of the benitoite group minerals and structural relations in (Si_3O_9) ring structure. Neues Jb. Miner., Mh., H.1, 16-30.

HAZEN, R.M., FINGER, L.W. & MARIATHASAN, J.W.E. (1985): High pressure crystal chemistry of scheelite-type tungstates and molybdates. *J. Phys. Chem. Sol.* **46**, 253-263.

HENDERSON, G.S. & FLEET, M.E. (1995): The structure of Ti silicate glasses by micro-Raman spectroscopy. *Can. Mineral.* **33**, 399-408.

HESS, P.C. (1991): The role of high field strength cations in silicate melts. *In* Physical Chemistry of Magmas (L.L.Perchuk & I. Kushiro, eds.). Springer-Verlag, New York, N.Y. (152-191).

HYBLER, J., PETŘÍČEK, V., JUREK, K., SKÁLA, R. & CÍSAŘOVÁ, I. (1997): Structure determination of vistepite $SnMn_4B_2Si_4O_{16}(OH)_2$: isotypism with bustamite, revised crystallographic data and composition. *Can. Mineral.* **35**, 1283-1292.

KEPPLER, H. & WYLLIE, P.J. (1991): Partitioning of Cu, Sn, Mo, W, U, and Th between melt and aqueous fluid in the systems haplogranite–H_2O–HCl and haplogranite–H_2O–HF. *Contrib. Mineral. Petrol.* **109**, 139-150.

KLEIN, S. & WEITZEL, H. (1976): Magnetische Struktur von $Mn(Nb_{0.5}Ta_{0.5})_2O_6$, Manganotantalit. *Acta Crystallogr.* **A32**, 587-591.

KOSSIAKOFF, A.A. & LEAVENS, P.B. (1976): The crystal structure of eakerite, a calcium–tin silicate. *Am. Mineral.* **61**, 956-962.

KRAUSE, M.O. & OLIVER J.H. (1979): Natural widths of atomic K-levels and L-levels, K-α x-ray-lines and several KLL auger lines. *J. Phys. Chem. Ref. Data* **8**, 329-338.

LÉGER, J.M. & HAINES, J. (1996): The high pressure behaviour of the cotunnite and post-cotunnite phases of $PbCl_2$ and $SnCl_2$. *J. Phys. Chem. Solids* **57**, 7-16.

LEHMANN, B. (1990): *Metallogeny of Tin*. Springer-Verlag, Berlin, Germany.

LINNEN, R.L. (1998): Depth of emplacement, fluid provenance and metallogeny in granitic terrains: a comparison of western Thailand with other Sn–W belts *Mineral. Deposita* **33**, 461-476.

LINNEN, R.L. (2005): The effect of water on accessory phase solubility in subaluminous and peralkaline granitic melts. *Lithos* **80**, 267-280.

LINNEN, R.L., PICHAVANT, M. & HOLTZ, F. (1996): The combined effects of fO_2 and melt composition on SnO_2 solubility and tin diffusivity in haplogranitic melts. *Geochim. Cosmochim. Acta* **60**, 4965-4976.

LINNEN, R.L., PICHAVANT, M., HOLTZ, F. & BURGESS, S. (1995): The effect of fO_2 on the solubility, diffusion and speciation of tin in haplogranitic melt at 850°C and 2 kbar. *Geochim. Cosmochim. Acta* **59**, 1579-1588.

LIU, Y. & NEKVASIL, H. (2002): Si–F bonding in aluminosilicate glasses: inferences from ab initio NMR calculations. *Am. Mineral.* **87**, 339-346.

LYTLE, F.W., GREEGOR, R.B., SANDSTROM, D.R., MARQUES, E.C., WONG, J., SPIRO, C.L., HUFFMAN, G.P. & HUGGINS, F.E. (1984): Measurement of soft X-ray absorption spectra with a fluorescent ion chamber detector. *Nucl. Instrum. Methods Phys. Res. A* **226**, 542-548.

MAKSIMOVA, I.V., ILUHIN, V.V. & BELOV, N.V. (1975): Crystal structure of thoreaulite, $SnTa_2O_6$. *Dokl. Akad. Nauk SSSR* **223**, 1115-1118 (in Russ.).

MAKSIMOVA, M. (1973): The crystal structure of sorensenite. *Dokl. Akad. Nauk SSSR* **213**, 91-93.

METCALF JOHANSEN J. & GRONBAEK HAZELL R. (1976): Crystal structure of sorensenite, $Na_4SnBe_2(Si_3O_9)_2(H_2O)_2$. *Acta Crystallogr.* **B 32**, 2553-2556.

MUKERJEE, S. & MCBREEN, J. (1999): An in situ X-ray absorption spectroscopy investigation of the effect of Sn additions

to carbon-supported Pt electrocatalysts I. *J. Electrochem. Soc.* **146**, 600-606.

MUSIC, S., BAJS, Z., FURIC, K. & MOHACEK, V. (1991): Mössbauer and vibrational spectra of sodium borosilicate glasses containing europium or tin ions (for radioactive waste immobilisation). *J. Mater. Sci. Lett.* **10**, 889-892.

MYSEN, B.O. (1990): Relationships between silicate melt structure and petrologic processes. *Earth Sci. Rev.* **27**, 281-365.

NASKI, G.G. & HESS, P.C. (1985): SnO_2 solubility: experimental results in peraluminous and peralkaline high silica glasses. *Trans. Am. Geophys. Union* (*Eos*) **66**, 412 (abstr.).

PANNETIER, J. & DENES, G. (1980): Tin(II) oxide: structure refinement and thermal expansion. *Acta Crystallogr.* **B36**, 2763-2765.

PAULING, L. (1929): The principles determining the structure of complex ionic crystals. *J. Am. Chem. Soc.* **51**, 1010-1026.

PICHAVANT, M., BOHER, M., STENGER, J.F., AÏSSA, M. & CHAROY, B. (1987): Relations de phase des granites de Beauvoir à 1 et 3 kbar en conditions de saturation en H_2O. *Géol. France* **2–3**, 77-86.

PIILONEN, P., FARGES, F. & LINNEN, B. (2002): The effects of peralkalinity on the structural environment of Nb and Ta in silicate glasses. *EMPG IX* (*Zürich*) *Conf. Abstr.* **5**(1), 85.

PIILONEN, P., FARGES, F., LINNEN, B. & BROWN, G.E., JR. (2005): Tin and niobium in dry and fluid-rich (H_2O, F) silicate glasses. *Phys. Scripta* **T115**, 405-407.

PIILONEN, P., FARGES, F., LINNEN, R.L., BROWN, G.E., JR., PAWLAK, M. & PRATT, A. (2006): Structural environment of Nb^{5+} in dry and fluid-rich (H_2O, F) silicate glasses: a combined XANES and EXAFS study. *Can. Mineral.* **44**, 775-794.

REYNARD, B. & WEBB, S.L. (1998): High-temperature Raman spectroscopy of $Na_2TiSi_2O_7$ glass and melt: coordination of Ti^{4+} and nature of the configurational changes in the liquid. *Eur. J. Mineral.* **10**, 49-58,1998.

SAYERS, D.E. (2000): Report of the International XAFS Society Standards and Criteria Committee. http://ixs.csrri.iit.edu/IXS/subcommittee_reports/sc

SEBY, F., POTIN-GAUTIER, M., GIFFAUT, E. & DONARD, O.F.X. (2001): A critical review of thermodynamic data for inorganic tin species. *Geochim. Cosmochim. Acta* **65**, 3041-3053.

SEKI, H., ISHIZAWA, N., MIZUTANI, N. & KATO, M. (1984): High temperature structures of the rutile-type oxides, TiO_2 and SnO_2. *Yogyo Kyokai Shi* (*J. Ceramic Assoc.*) **92**, 219-223.

SHANNON, R.D. & PREWITT, C.T. (1969): Effective ionic radii in oxides and fluorides. *Acta Crystallogr.* **B25**, 925-945.

SHERMAN, D.M., RAGNARSDOTTIR, K.V., OELKERS, E.H. & COLLINS, C.R. (2000): Speciation of tin Sn and Sn in aqueous Cl solutions from 258 to 350°C: an in situ EXAFS study. *Chem. Geol.* **167**, 169-176.

SUBBOTIN, V.V., MERLINO, S., PUSHCHAROVSKII, D.YU., PAKHOMOVSKII, YA.A., FERRO, O., BOGDANOVA, A.V., VOLOSHIN, A.V., SOROKHTINA, N.V. & ZUBKOVA, N.V. (2000) Tumchaite $Na_2(Zr_{0.8}Sn_{0.2})Si_4O_{11}(H_2O)_2$ – a new mineral from carbonatites of the Vuoriyarvi alkali-ultrabasic massif, Murmansk region, Russia. *Am. Mineral.* **85**, 1516-1520.

TAYLOR, J.R. & WALL, V.J. (1992): The behavior of tin in granitoid magmas. *Econ. Geol.* **87**, 403-420.

TAYLOR, R.G. (1979): *Geology of Tin Deposits*. Elsevier, Amsterdam, The Netherlands.

TISCHENDORF, G. (1977): Geochemical and petrographic characteristics of silicic magmatic rocks associated with rare element mineralization. *In* Metallization Associated with Acid Magmatism (MAWAM) **2**. (M. Stemprok, L. Burnol & G. Tischendorf, eds.). Czech Geological Survey, Prague, Czech Republic (41-96).

VALLET-REGI, M., GONZALES-CALBET, J.M., ALARIO-FRANCO, M.A. & VEGAS, A. (1986): The $ASnO_3$ (A = Ca, Sr) perovskites. *Acta Crystallogr.* **C42**,167-172.

WIDERA, A. & SCHAEFER, H. (1981): Das Zustanddiagramm Sr–Sn und die Verbindung Sr_3SnO. *J. Less-Common Metals* **77**, 29-36.

WINDY, J.L. & DRAKE, M.J. (2000): Metal–silicate partitioning of Co, Ga and W; dependence on melt composition. *Geochim. Cosmochim. Acta* **64**, 3887-3895.

WINTERER, M. (1997): The XAFS package. *J. Phys. IV, Colloq.* **7–C2**, 243-244.

ZENG, Q. & STEBBINS, J.F. (2000): Fluoride sites in aluminosilicate glasses: high-resolution ^{19}F NMR results. *Am. Mineral.* **85**, 863-867.

Received November 24, 2004, revised manuscript accepted November 22, 2005.